Energy 225 (2021) 120245

Contents lists available at ScienceDirect

Energy

journal homepage: www.elsevier.com/locate/energy

Study on thermal performance of a PCM enhanced hydronic radiant floor heating system

Barbara Larwa*, Silvia Cesari, Michele Bottarelli

Department of Architecture, University of Ferrara, Via Quartieri 8, Ferrara, 44121, Italy

ARTICLE INFO

Article history:
Received 15 September 2020
Received in revised form
24 February 2021
Accepted 27 February 2021
Available online 4 March 2021

Keywords:
Phase change materials (PCMs)
Radiant floor
Thermal energy storage
Experimental testing
Numerical modelling

ABSTRACT

Radiant floor systems enhanced with Phase Change Materials (PCMs) could achieve significant energy savings while improving the thermal comfort of occupants in lightweight buildings. Effective integration of PCMs typically requires customised solutions based on a comprehensive analysis due to their complex nature. The objective of the present study is the experimental and numerical investigation of a hydronic radiant floor heating system integrated with macroencapsulated PCM. Experimental tests were carried out on a laboratory-scale by the University of Ferrara, Italy, within the H2020 European project IDEAS. A 2D model was then implemented in COMSOL Multiphysics and calibrated in steady as well as in transient state according to the experimental tests. The behaviour of the system, including temperature distribution and heat flux, were analysed under different conditions. The impact of using dry and wet sand, as well as the effect of the position of PCM – above or under heating pipes – on thermal performance, were investigated. Results showed that the use of high thermal conduction in mortar increases much faster the overall performance of the PCM integrated underfloor heating system. Furthermore, the coupling technology with PCM containers installed under piping significantly enhances the positive effect of wet sand.

1. Introduction

Despite space heating energy consumption in the service sector is decreasing rapidly with the improvement of the energy performance of buildings – accounting for 46% of total energy use against 63% in 1990 – it still represents a considerable share of household energy consumption, equal to about 67%, as well as a substantial fraction of greenhouse gas emissions [1]. For this reason, new design strategies for radiant heating floor systems are being widely investigated.

Underfloor heating systems use lower temperature sources in comparison with conventional systems. Furthermore, by directly heating the floor surface they ensure a uniform temperature distribution which improves indoor thermal comfort. This technology is also suitable for the majority of generators, in particular, heat pumps and boilers, and can be operated with various sources of renewable energy. Nevertheless, significant energy performance and optimal thermal comfort may not be achieved when underfloor heating is adopted in lightweight buildings. Indeed, despite being widely employed for economic reasons, these types of envelope are characterised by a low thermal capacity.

Radiant floor systems integrated with Phase Change Materials (PCMs) allow obtaining significant energy savings while improving indoor thermal comfort in lightweight buildings [2,3]. PCMs can store or release a large quantity of thermal energy by using latent heat during the phase change process as a kind of thermal storage material in building applications. Therefore, the use of PCMs is an efficient way to increase the thermal inertia of building envelopes, thus reducing temperature fluctuations and leading to the improved thermal comfort of occupants [4].

A growing body of literature investigated water-based radiant floor heating systems integrated with PCMs in dry and wet construction [5–13]. However, PCM-related theoretical and validation research is still in its early stages. More in detail, there is a lack of worthy studies that experimentally investigated the energy performance of macroencapsulated PCM enhanced by sand in hydronic radiant floors. In Barrio et al. [14], sand was considered as sensible heat storage material instead of concrete for comparison with PCM, but its role combined with PCM was not examined. Zhou and He [15] compared the thermal performance of polyethylene

* Corresponding author.
E-mail address: barbara.larwa@unife.it (B. Larwa).

https://doi.org/10.1016/j.energy.2021.120245

(PE) pipes and macroencapsulated inorganic PCM (melting point 29 °C) with capillary mat and sand. The former floor structure consisted of a 16 mm thick wood board as finishing, 6 mm PCM layer (sand in the latter floor configuration), heating pipes (capillary mat in the latter floor configuration), 50 mm thick polystyrene and 120 mm thick reinforced concrete. However, similarly to in Barrio et al. [14], sand was considered only as a thermal mass layer to be compared to PCM. Baek and Kim [16] carried out a numerical analysis of a water-based radiant floor integrated with PCM in containers placed under heating pipes. The system was composed as follows: 40 mm finishing mortar with pipes installed on the bottom, 15 mm PCM within two layers of 10 mm mortar, 20 mm insulation, and 210 mm concrete slab. PCM was encapsulated within a very thin aluminium film and was characterised by a melting point of 44 °C. It was found that assuming a supply water temperature of 40 °C, the average floor surface temperature was 30 °C. It should be noted that 29 °C is the maximum value of floor surface temperature allowed by regulation in typically occupied areas with a heating setpoint temperature of 20 °C [17]. Park and Kim [18] tested the thermal performance of a n-paraffin PCM with a melting point of 42 °C in thin-film aluminium packaging. The floor structure was the same as in Ref. [16] except for PCM, which was 10 mm thick and was comprised between two layers of 15 mm mortar. Considering a supply water temperature of 55 °C, it was observed that the average floor surface temperature reached 32 °C during operation – therefore decisively higher than the regulatory limit – and it was still nearly 30 °C after 12 h since the shutdown of the system, with an indoor air temperature of about 29 °C. Lu et al. [19] carried out experimental tests on a double pipe PCM floor heating system. The floor consisted of the following layers: 40 mm dry hard cement mortar and floor tile, 200 mm cement mortar as filling layer with PCM integrated pipes installed on the bottom, 50 mm insulation, 50 mm cement board. A paraffin PCM with a melting point of 36 °C, a supply water temperature of 50 °C, and pipe diameter of 32 mm were considered in the test. Results showed that the floor surface temperature ranged from 22 to 29 °C, heat flux through floor surface varied from 16 to 67 W/m^2. In the following study [20] the same floor structure and conditions were assumed to conduct a numerical analysis and optimisation of PCM encapsulated by PE casing pipes. Optimal parameters to achieve indoor thermal comfort were found to be pipe pitch of 28 cm and thickness of PCM equal to 2 cm. Plytaria et al. [21] compared the thermal performance of PCM installed under and above heating pipes in an underfloor solar-assisted heating system. For PCM-under-pipes scenario, the floor was composed of 10 mm finishing mortar, 60 mm concrete with pipes installed inside, 14 mm PCM layer, 50 mm insulation, and 200 mm concrete slab. In the second scenario the PCM layer was set between finishing mortar and 60 mm concrete with pipes. A PCM melting point of 29 °C and supply water temperature of 40 °C were considered. The pitch and diameter of pipes were 10 cm and 2 cm respectively. The heating setpoint temperature was 22 °C. Findings showed that the PCM layer under water pipes allowed to have the best room temperature fluctuation and ensured indoor thermal comfort with lower energy consumption.

The review of the existing studies presented above underlines that successful integration of PCMs typically requires customised solutions based on a comprehensive analysis both numerical and experimental due to their complex nature [22,23].

Against this background, the H2020 European project IDEAS – Novel building Integration Designs for increased Efficiencies in Advanced Climatically Tunable Renewable Energy Systems – [24] is focused on the development of a novel low-cost building integrated RES which will cost-effectively exceed current RES efficiencies, generating electricity, heat, and cooling and that will be optimised in different climatic conditions. More in detail, the work package n.3 (WP3 leader: UNIFE - University of Ferrara, Italy) aims to design a multi-source heat pump (HP) system able to balance the non-synchronous energy matching between renewable energies (sun, ground, air) and energy demands for space heating and cooling by means of innovative devices enhanced with PCMs.

The integration of PCMs in a radiant floor system as a technology for space heating and cooling was investigated by UNIFE through numerical and experimental investigation. The most suitable solution was then installed in a first prototype at a small-scale in an existing experimental building in Ferrara.

The aim of this study is the numerical and experimental analysis of a hydronic radiant floor heating system enhanced with hydrated salts as PCM. The behaviour of the radiant floor system enhanced with suitable PCM – including temperature distribution and heat flux – were examined in order to check the benefits of PCMs when off the heating system. The impact of using dry and wet sand, as well as the effect of the position of PCM – above or under heating pipes – on thermal performance, were investigated.

2. PCM selection for the radiant floor

The WP3 aims to integrate HP technology for space heating and cooling via an Intra-day/season Thermal Energy Storage (ITES) and a Multi-source/sink Energy Sub-system (MES). MES was designed according to the functionality of an invertible heat pump able to exploit different thermal sources/sinks: sun, air (outdoor and waste heat), and ground. ITES represents the thermal buffer to equilibrate different and non-synchronous thermal energy requirements. At seasonal and building footprint, the ITES functionality can be supplied by means of horizontal ground heat exchangers coupled with PCMs. At building and daily scale, the function can be provided by an underfloor heating/cooling system and by a novel PV/T solution, all enhanced with suitable PCMs.

A small-scale prototype of the IDEAS plant was installed in TekneHub laboratory of UNIFE, involving the selection of proper PCMs for each component, as well as of the coupling technology. The layout of the small-scale plant installed is illustrated in Fig. 1.

In order to identify the most suitable PCMs to enhance the energy performance of a hydronic radiant floor several evaluations, experimental and numerical analysis were carried out. The issue was initially faced with the assessment of the energy needs of the mock-up building, experimentally and by means of the relevant regulation.

2.1. Heating energy needs of the mock-up

Energy needs for space heating of the mock-up (Fig. 2) were assessed based on monitoring data collected by thermal meters installed at the fan coils inlets/outlets. One typical day of the heating period, from January 10th, 2020 at 9:49 a.m. to January 11th, 2020 at 9:48 a.m. was considered, with volumetric airflow of fan coils equal to 140 m^3/h. As regards outdoor and indoor environmental conditions, outdoor air temperatures were acquired by the weather station installed outside the mock-up in Ferrara, while indoor heating set point temperature was set equal to 20 °C.

A first elaboration of the main measurement data is reported in Table 1. Graphical data of the thermal monitoring of the mock-up is shown in Fig. 3. Here, values of outdoor air temperature (orange line), instantaneous power of the fan coils (red line) and the related thermal energy required to meet the mock-up heating energy demand (blue line) are reported for the 24-h period examined. Throughout the monitoring, instantaneous power of the fan coils did not exceed 3 kW, except for a single peak at around 22:00; average instantaneous power resulted to be equal to 0.497 kW. The

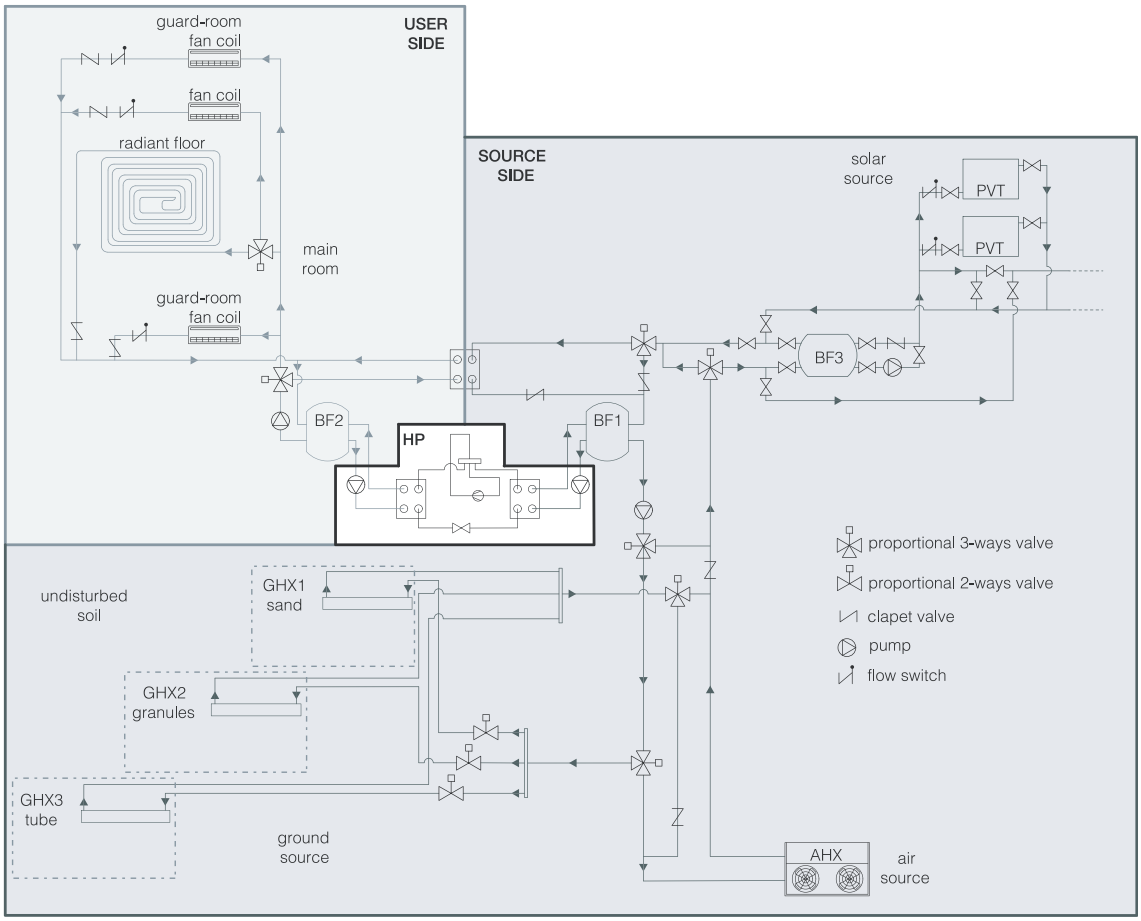

Fig. 1. Layout of the small-scale plant installed.

Fig. 2. Mock-up.

total thermal energy needed to provide space heating and maintain a setpoint temperature of 20 °C during the 24-h period monitored was equal to 11.92 kWh.

Considering a conditioned floor area of the room (where the radiant floor was installed) of 13 m^2, and a conditioned volume of 31.2 m^3 (internal height of 2.4 m), the values outlined in Table 1 allowed to identify average energy needs, as reported in Table 2.

Table 1
Thermal monitoring of the mock-up (from Jan. 10 (9:49 a.m.) to Jan. 11 (9:48 a.m.), 2020): summary of the results.

Parameter	Value	Unit
Time ON	11.4	hours
Daily energy for heating (20 °C)	11.92	kWh
Daily average power when ON	1.043	kW
Daily average power	0.497	kW
Average flow rate when ON	307.4	l/h

Furthermore, based on the time series presented in Fig. 3, the charts reported below were obtained (Figs. 4 and 5). The former illustrates the relation between the operating minutes of the fan coil and outdoor air temperature, always considering a heating setpoint temperature of 20 °C. In the latter, the daily average thermal power of the fan coil is analysed in relation to the difference between the heating setpoint temperature and outdoor air temperature.

The energy performance analysis of the building envelope allowed to evaluate the energy demand of the mock-up in steady-state as:

$$U_{wall} = \frac{1}{\frac{1}{20} + \frac{0.12}{0.06} + \frac{1}{10}} = 0.465 \ \frac{W}{(m^2K)} \quad (1)$$

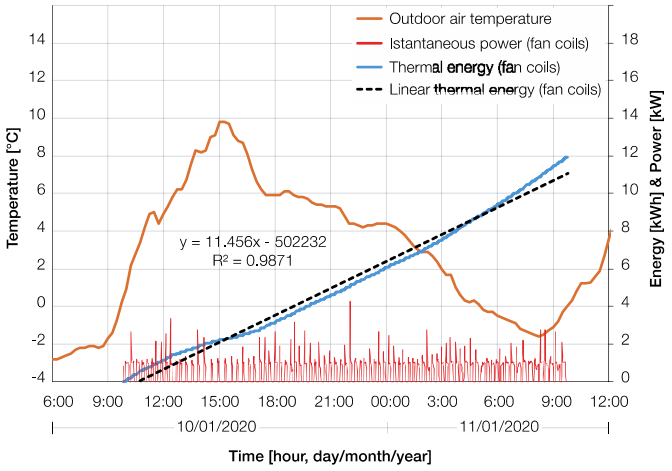

Fig. 3. Thermal monitoring of the mock-up, from Jan. 10 (9:49 a.m.) to Jan. 11 (9:48 a.m.), 2020.

Table 2
Average power and energy needs of the mock-up.

Parameter	Value	Unit
Daily average power per unit volume	15.9	W/m^3
Daily average power per unit area	38.2	W/m^2
Average power when ON per unit volume	33.5	W/m^3
Average power when ON per unit area	80.2	W/m^2
Daily average energy demand per unit volume	0.382	kWh/m^3
Daily average energy demand per unit area	0.917	kWh/m^2

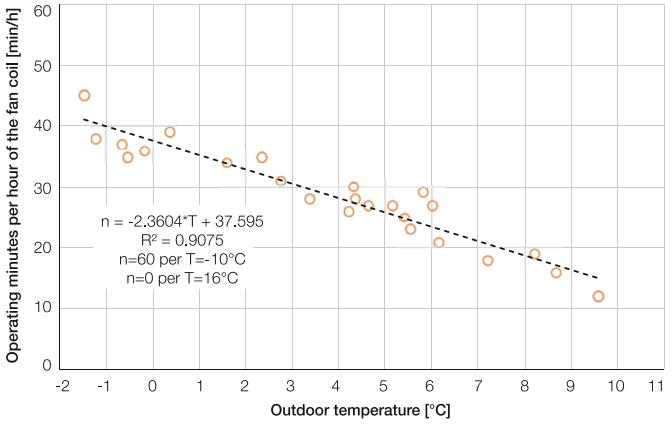

Fig. 4. Fan coil operating minutes vs. air temperature.

$$U_{roof} = \frac{1}{\frac{1}{10} + \frac{0.07}{0.6} + \frac{0.03}{0.1} + \frac{1}{10}} = 1.62\ \frac{W}{(m^2K)} \tag{2}$$

$$\dot{Q} = \sum A_i U_i \cdot \Delta T \tag{3}$$

$$\sum A_i U_i = 56.8\ \frac{W}{K} \tag{4}$$

Therefore, the rough factor of 57 W/K was assumed as the heating energy demand of the mock-up per unit degree of difference between the heating setpoint temperature and the outdoor air temperature. For the sake of completeness, values for surface and thermal transmittance of the components of the building envelope are reported in Table 3.

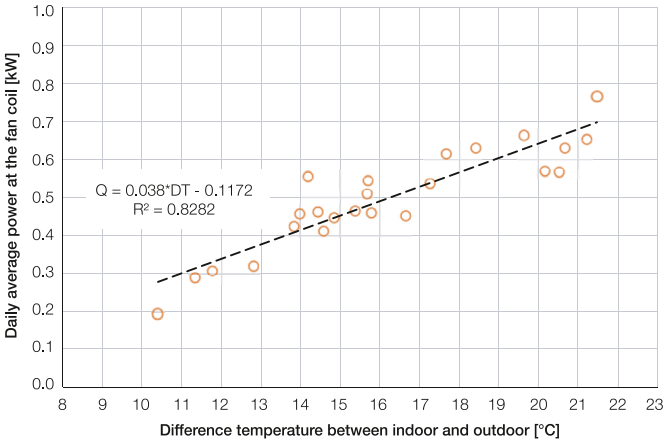

Fig. 5. Daily average thermal power of the fan coil vs. difference between indoor (20 °C) and outdoor air temperature.

Fig. 6 represents the time series of outdoor air temperature during winter 2018–2019 (heating season defined by regulation is from October 15th to April 15th) collected at the TekneHub laboratory, in relation to the heating energy needs per unit conditioned floor area of the mock-up. Heating energy demand was parametrically assessed by multiplying the rough factor of 57 W/K by the difference between the heating set point temperature and the outdoor air temperature. The analysis of the chart underlines that specific heating energy demand was rarely greater than 60 W/m^2.

The cumulative frequency of the heat flux per unit conditioned floor area is showed in Fig. 7. Here, energy demand is approximatively met with a heat flux of 30 W/m^2 for 50% of the heating period.

Considered that the first function of the PCM integrated into the radiant floor is to provide heating when the control unit makes the heat pump turns off, the value of heat flux mentioned before (30 W/m^2) was assumed as the reference value for the selection of the PCM melting point. Indeed, heat flux values higher than 30 W/m^2 are related to higher temperatures of the working fluid as well as to higher PCM melting points. This would be decisively excessive and not adjustable when the mock-up is characterised by lower energy needs.

2.2. Radiant floor design according to standard regulation

The heat flow between heating pipes and the environment for the radiant floor structure as depicted in Fig. 8 is calculated according to the *European Standard EN ISO 11855-2:2012. Building environment design - Design, dimensioning, installation, and control of embedded radiant heating and cooling systems - Part 2: Determination of the design heating and cooling capacity* [25] with the following equation:

$$q = B \cdot \prod_i \left(a_i^{m_i}\right) \cdot \Delta\theta_H \tag{5}$$

where B is a coefficient that depends on the system; $\prod_i (a_i^{m_i})$ is the product that connects the parameters of the structure; $\Delta\theta_H$ is the logarithmic mean temperature difference between the fluid and the environment.

Table 3
Building physics.

Parameter	Value	Unit
Wall surface (4 × 4.7 × 2.4)	45.1	m^2
Roof surface (4.7 × 4.7)	22.1	m^2
Floor surface (4.7 × 4.7)	22.1	m^2
Wall thickness	0.12	m
Wall thermal conductivity	0.06	W/(mK)
Deck thickness at the roof	0.03	m
Deck thermal conductivity	0.1	W/(mK)
Gravel layer thickness on the roof	0.07	m
Gravel layer thermal conductivity	0.6	W/(mK)
Inner convective heat transfer coefficient for wall	10	$W/(m^2K)$
Outer convective heat transfer coefficient for wall	20	$W/(m^2K)$
Upper convective heat transfer coefficient for roof	10	$W/(m^2K)$
Lower convective heat transfer coefficient for roof	10	$W/(m^2K)$

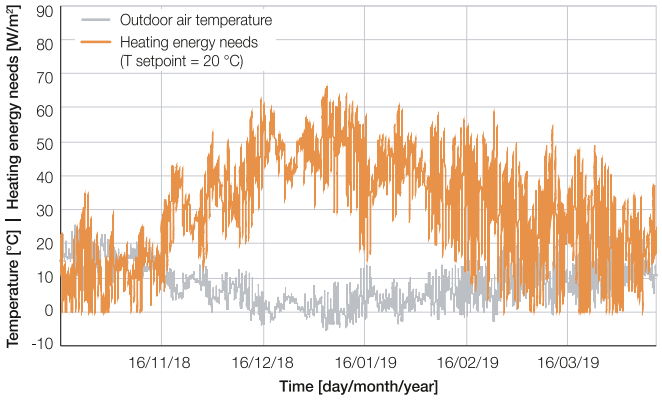

Fig. 6. Time series of air temperature and corresponding heat flux for heating mode in winter 2018–2019.

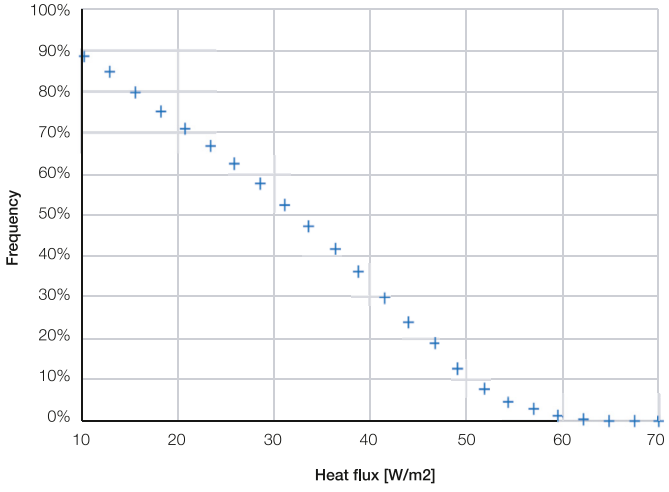

Fig. 7. Cumulative frequency of heat flux in heating mode. Radiant floor design according to standard regulation.

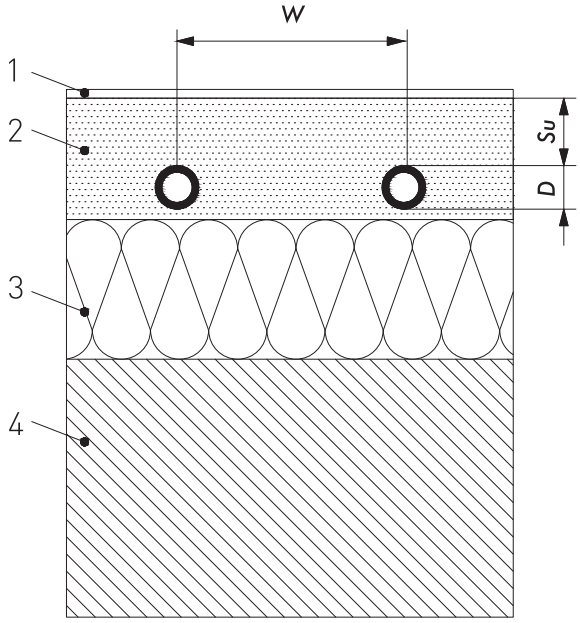

Fig. 8. Radiant floor structure: 1) floor finishing, 2) mortar, 3) thermal insulation, 4) concrete slab [25].

In particular, B is equal to 6.7 $W/(m^2K)$ if the thermal conductivity of the pipe is $\lambda_R = 0.35$ W/(mK), and the thickness of the pipe is $s_R = 0.002$ m.

The logarithmic mean temperature is calculated as:

$$\Delta\theta_H = \frac{\theta_V - \theta_R}{ln\frac{\theta_V - \theta_i}{\theta_R - \theta_i}} \tag{6}$$

where θ_V and θ_R are the inlet and outlet temperature of the heat transfer fluid respectively; θ_i is the setpoint temperature of the room.

Finally, the product is calculated with the following equation:

$$\prod_i \left(a_i^{m_i}\right) = a_B \cdot a_W^{m_W} \cdot a_U^{m_U} \cdot a_D^{m_D} \tag{7}$$

where a_B is the surface coating factor, which is evaluated as:

$$a_B = \frac{\frac{1}{\alpha} + \frac{s_{u,0}}{\lambda_{u,0}}}{\frac{1}{\alpha} + \frac{s_{u,0}}{\lambda_E} + R_{\lambda,B}} \tag{8}$$

where:

$\alpha = 10.8$ $W/(m^2K)$;
$\lambda_{u,0} = 1.0$ W/(mK);
$s_{u,0}$: thickness above the pipe, equal to 0.045 m;
$R_{\lambda,B}$: thermal resistance of the floor finishing, it must not exceed the value of 0.15 $(m^2K)/W$. For example, ceramic tiles are characterised by $R_{\lambda,B} = 0.012$ $(m^2K)/W$;
λ_E: thermal conductivity of the mortar, equal to 1.2 W/(mK);

Table 4
Design temperatures.

	Winter	Summer	Unit
θ_V	35	15	°C
θ_R	32	20	°C
θ_i	20	26	°C

a_W: piping pitch factor, $a_W = f(R_{\lambda,B})$, to know the progress of the function, refer to table A1 of the EN ISO 11855 standard;
a_U: coating factor, $a_U = f(W, R_{\lambda,B})$, to know the progress of the function, refer to table A2 of the EN ISO 11855 standard;
a_D: external diameter of the pipe factor, $a_D = f(W, R_{\lambda,B})$, to know the progress of the function, refer to table A3 of the EN ISO 11855 standard;
W: piping pitch;
D: outside diameter of the pipe;
m_W: 1 - *W*/0.075;
m_U: 100·(0.045 - s_u), with s_u thickness above the pipe;
m_D: 250·(*D*-0.020).

In order to calculate the progress functions necessary to evaluate the parameters a_W, a_U, a_D, intermediate values, extrapolated from the tables A1, A.2, A.3 of the EN ISO 11855 standard, must be interpolated using a natural cubic spline function.

Design temperatures are presented in Table 4, while heat flow results in relation to the logarithmic mean temperature $\Delta\theta_H$ are reported in Table 5.

The results of this simplified calculation showed that a heat flux equal to almost 70 W/m^2 was required to maintain a setpoint temperature of the room of 20 °C during the winter season. During the cooling period, instead, when the room setpoint temperature was 26 °C, a heat flux of 10 W/m^2 was necessary.

As already mentioned in section 2, the selection of suitable PCM was conducted also based on an accurate numerical analysis, which produced results characterised by higher values than those obtained analytically. This discrepancy is since the calculation method used by COMSOL is certainly more accurate than the method used by the standard EN ISO 11855, which proposes a simplified calculation procedure that is precautionary too.

2.3. Remarks

A large number of simulations of the behaviour of the radiant floor system integrated with hydrated salt as PCM were carried out by considering different melting temperatures, to identify the most effective ones for the heating and the cooling season.

Results showed that the selection of a PCM with a melting point of 27 °C for heating purposes was better and justified as it allowed to meet heating energy needs of the mock-up building and, by adopting a supply water temperature of 35 °C, it allowed to obtain the best thermal efficiency. The same value of water temperature was found to achieve the most significant energy savings in Mohammadzadeh and Kavgic [2]. Moreover, by considering a temperature of 35 °C for water, floor surface temperature was nearly 29 °C, which is the maximum value allowed by regulation in typically occupied areas with a setpoint temperature of 20 °C [17].

Table 5
Heat flow results in relation to $\Delta\theta_H$.

	Winter	Summer	Unit
$\Delta\theta_H$	13.4	35.0	°C
q	68.6	−9.6	W/m^2

For cooling purposes, it was found that a suitable and reasonable choice was a PCM with a melting temperature of 21 °C, as already demonstrated by other studies in literature [26–28]). Indeed, a PCM melting point centred around the human comfort temperature contributes to preventing the surface condensation problems that often occur when standard radiant floors are used for cooling [29–31].

More in detail, PCMs S27 and S21 provided by PCM Products Ltd. [32], partner of IDEAS European project, were selected. As for the coupling technology with the radiant floor system, PCMs were encapsulated in thin high-density polyethylene (HDPE) containers so called ThinICE provided by the same company.

3. Methods

The behaviour of the radiant floor system enhanced with selected S27 as PCM was examined in order to check the benefits of PCMs. The impact of using wet and dry sand on the thermal performance of the system, along with the effect of PCM containers position (above and under the piping) were investigated. Experimental tests were carried out in a laboratory scale in TekneHub laboratory of the University of Ferrara (UNIFE), Italy.

3.1. Experimental tests

3.1.1. Experimental setup

The radiant floor system realised in the experimental tests and then implemented in COMSOL Multiphysics consists of a few different layers as illustrated in Figs. 9 and 10: thin wooden layer as floor finishing, dry/wet sand as filling material, PCM layer, dry sand and two layers of Expanded Polystyrene insulation (EPS).

As already mentioned in section 2.3, PCM was encapsulated in thin HDPE containers installed under/above heating pipes. Low-density polyethylene (LDPE) pipes (thermal conductivity 0.35 W/mK) with external diameter of 16 mm and wall thickness 2 mm were placed in sand layer with a distance of 80 mm. The adopted configuration for radiant floor is not standard but was defined based on the next experimental installation in the small-scale prototype in which thickness constraints were imposed; moreover, the use of sand as plenum was proposed to have the chance for maintenance and replacement of PCM containers.

Thermal properties of each layer composing the radiant floor are outlined in Table 6. Thermal properties of the selected PCM are reported in Table 7.

As showed in Fig. 11, the radiant floor tests were realised into an OSB wooden container characterised by a 14 mm thickness. Working fluid (water) was provided employing Thermo Fisher Scientific ARCTIC A25 AC200 refrigerated bath circulator [37], with a supply temperature of 35/40 °C.

3.1.2. Measurement system

As depicted in Figs. 9 and 10, two heat flux meters [38] were installed below the floor finishing (HFM1) and above the insulation layer (HFM2) in order to measure heat flux. Using the known thermal characteristics of the heat flow plate and the thermo-electrically measured temperature gradient inside the heat flow plate the ALMEMO measuring system could thus measure the heat flow density in [W/m^2]. For temperature measurement, T-type thermocouples [39] with ALMEMO connectors [40] were positioned at the following interfaces, as illustrated in Figs. 9 and 10:

- air-floor finishing (T1);
- floor finishing-dry/wet sand (T2);
- dry/wet sand-PCM container (T3);
- PCM container-dry sand (T4);

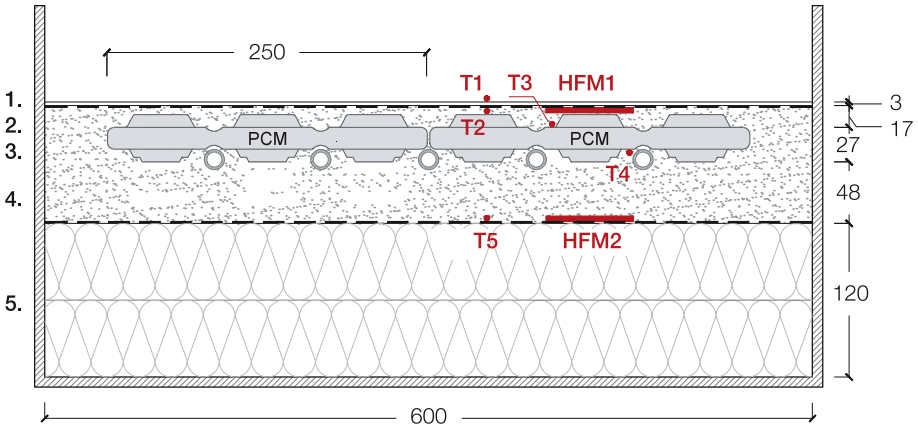

Fig. 9. Radiant floor configuration 1 (layer thickness expressed in mm) and sensors location.

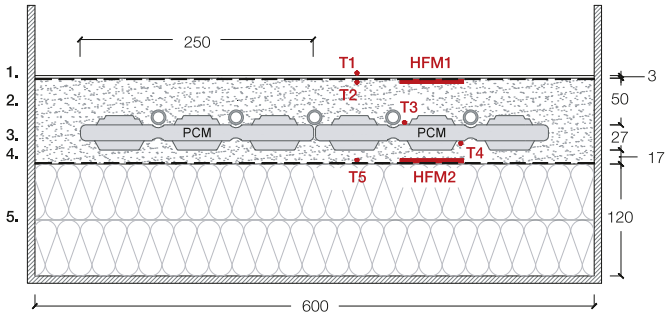

Fig. 10. Radiant floor configuration 2 (layer thickness expressed in mm) and sensors location.

- dry sand-insulation layer (T5).

Furthermore, two T-type thermocouples with ALMEMO connector were installed at the inlet and outlet of hot water loop to measure supply and outlet water temperature, and another one was employed for monitoring indoor air temperature. Data were acquired by ALMEMO 5690-2 M data logger [41]. Technical data of the heat flux meters and the thermocouples with ALMEMO connectors are reported in Tables 8 and 9. Uncertainties of used T-type thermocouples are reported in Table 10. The estimated uncertainty of used heat flux plates is equal ±1.3 W/m^2 for dry sand conditions and ±1.6 W/m^2 for wet sand conditions.

3.1.3. Test procedure

Experimental tests were conducted for two different conditions of the sand layer between floor finishing and PCM containers, dry and wet sand, to investigate the behaviour of the system implemented with low and high thermal conductivity respectively. Moreover, the impact of PCM container position was analysed – above (configuration 1) or under (configuration 2) the pipes. Two supply water temperatures were assumed, for a total of five different scenarios examined, as outlined in Table 11. Each experimental test was conducted for about six days. A slowly blowing fan was placed 2 m far from the setup in wet condition; a nylon sheet between sand and floor finishing and another one above insulation were used to avoid evaporation.

During the first days of experiment the system was continuously on to achieve steady state conditions, then it was turned off and its energy performance was analysed for the following days. The tests were carried out into a room where space heating was provided with fan coils maintaining an indoor air temperature of about 20–21 °C.

3.2. Numerical modelling

A 2D model of the radiant floor setup was implemented in the commercial finite element method (FEM) code COMSOL Multiphysics® 5.5 [42]. The model was calibrated in steady as well as in transient state according to the experimental tests and then it was used to analyse different configurations and thermal properties. A view of the geometry of the model is illustrated in Fig. 12.

To minimize the numerical errors and to expedite the computation, the size of the finite elements was chosen to be fine for the

Table 6
Floor structure materials and their thermophysical properties.

Material	Density kg/m^3	Specific heat J/(kgK)	Thermal conductivity W/(mK)
1. Wooden finish [33]	750	2300	0.400
2. Dry/wet sand [34]	1600/1900	900/1900	0.800/2.200
3. PCM [35]	1530	2200	0.540
4. Dry sand	1600	900	0.800
5. EPS insulation [36]	30	1450	0.034

Table 7
Thermal properties of the selected PCM S27 [35].

Melting temperature °C	Temperature range of transition °C	Density kg/m^3	Specific heat J/(kgK)	Latent heat kJ/(kg)	Thermal conductivity W/(mK)
27	26–31	1530	2200	185	0.54

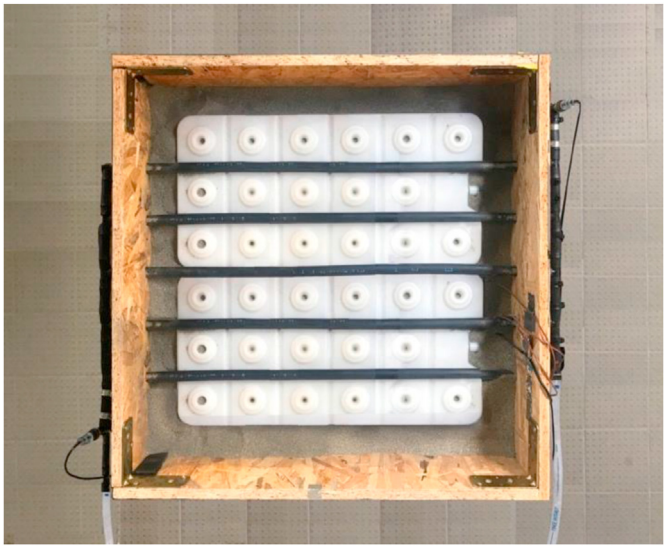

Fig. 11. Top view of the setup.

area close to the PCM containers and coarse for the area far from it. The full mesh is showed in Fig. 13 and it is limited to 21,949 elements to reduce the computational time. A number of 10,024 elements are reserved for the PCM layer with 2 mm maximum element size. To check the mesh independence of the solutions, the same problem in steady state case was solved with a mesh increased to more than 45,000 elements, and it was found there is a negligible change in the numerical solution.

Thermal properties and thickness of the radiant floor layers set in COMSOL are outlined in Tables 6 and 7

To control and drive the thermo-physical properties of PCM during the phase change the functions $H_i(T)$ and $D_i(T)$ were introduced, based on [43]. The PCM problem was numerically approached as simply porous media, which was composed by the two phases of the same material (solid, liquid). The specific heat capacity c_p was defined to consider the latent heat of fusion h^{SL} using a normalised Dirac's pulse $D(T)$ [K^{-1}]. Moreover, the phase change between the liquid phase (^{L}) and the solid one (^{S}) was expressed in Ref. [44] as a function of a dimensionless variable $H(T)$ which is the volumetric fraction of the liquid phase in a PCM, ranging between 0 and 1 concerning the temperature and changing around the melting point ($T_m \pm \Delta T$). These functions were introduced to moderate the switching between solid ($H(T_m\text{-}\Delta T) = 0$) and liquid phase ($H(T_m + \Delta T) = 1$) [45]. Thermal properties of the PCM during the phase change process were calculated on the basis of the equations reported in Ref. [45]. The $H_i(T)$ and $D_i(T)$ functions for PCM are depicted in Fig. 14.

As an initial condition, a constant temperature of 17 °C was assumed. Indoor air temperature of the room was considered equal to 20 °C both in steady state and in transient mode. On the outer surface of wooden floor finish and surface of the radiant floor a convection heat transfer as boundary condition was assumed. A value of heat transfer coefficient of 10 or 15 W/(m^2K) was considered on the surface of the radiant floor, due to operation of the fan in the room. A value of heat transfer coefficient of 10 W/(m^2K) was considered when a slowly blowing fan was turned off and a value equal to 15 W/(m^2K) was used when the fan was turned on.

Table 9
Technical data of the T-type thermocouples [39].

Variant with thermal material	Measurement Range °C	Accuracy °C
Cu–CuNi (T)	−200 to +350	0.5

Table 10
Uncertainties of used T-type thermocouples.

Thermocouple	Value °C
T1	±0.170
T2	±0.180
T3	±0.191
T4	±0.189
T5	±0.187
T (inlet)	±0.188
T (outlet)	±0.189

Table 11
Scenarios investigated in experimental tests.

Radiant floor configuration	Sand condition	Supply water temperature °C
1	dry	35
1	wet	40
1	wet	35
2	dry	35
2	wet	35

4. Results and discussion

4.1. Experimental tests – configuration 1

4.1.1. Dry sand condition

Time series of temperatures and heat fluxes for the dry sand condition are illustrated in Fig. 15. During the first part of the test,

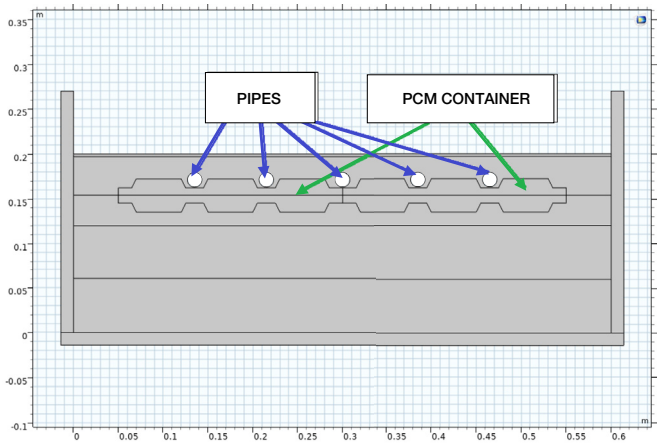

Fig. 12. Sketch of the model domain implemented in COMSOL – configuration 2.

Table 8
Technical data of the heat flow plates [38].

Dimensions mm	Meander Size mm	Substrate	Temperature Stability °C	Accuracy of calibration value
120 × 120 × 1.5	90 × 90	epoxy resin	−40 … +80	5% at 23 °C

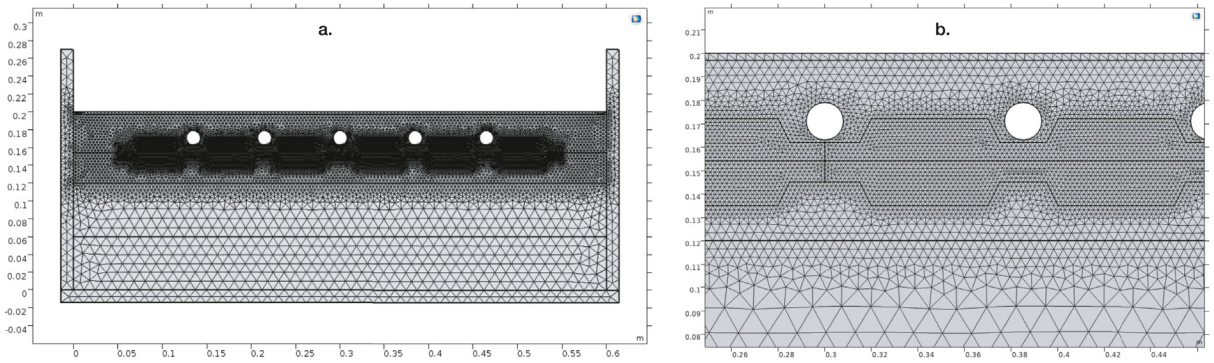

Fig. 13. Sketch of the mesh: whole domain (a) and focus (b) – configuration 2.

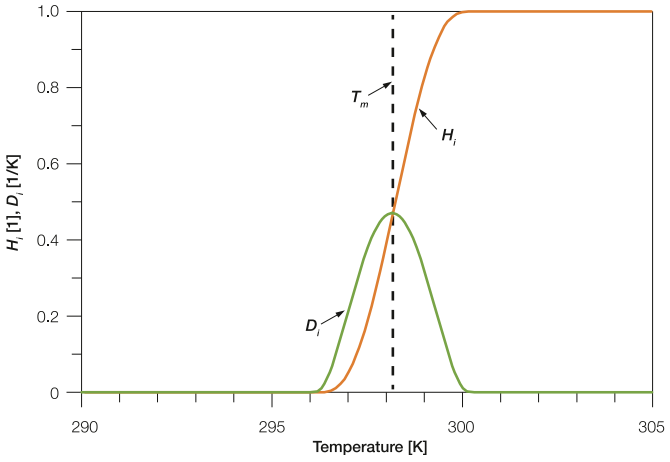

Fig. 14. H_i and D_i functions defining the phase change of the PCM.

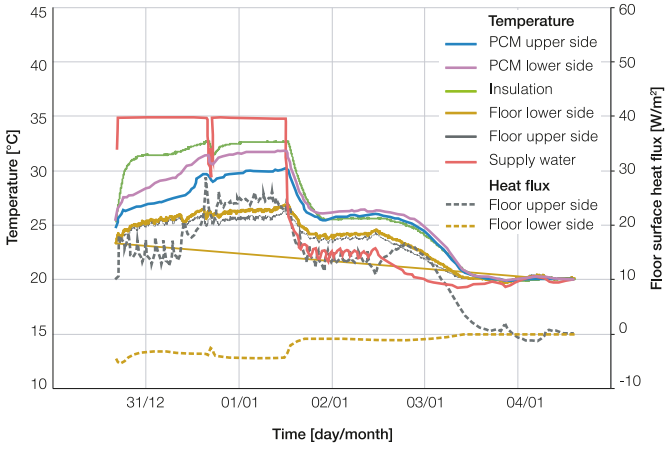

Fig. 15. Temporal changes in temperature and heat flux in dry sand condition, 35 °C supply water temperature (configuration 1).

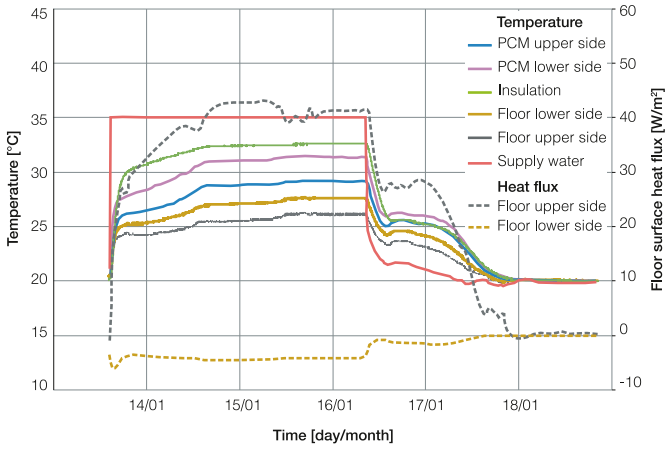

Fig. 16. Temporal changes in temperature and heat flux in wet sand condition, 35 °C supply water temperature (configuration 1).

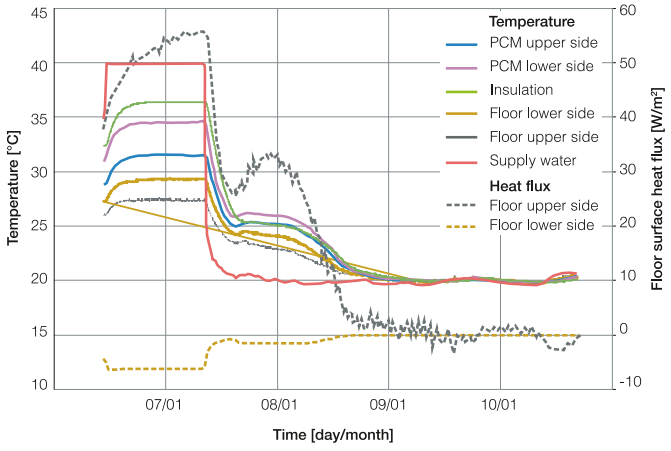

Fig. 17. Temporal changes in temperature and heat flux in wet sand condition, 40 °C supply water temperature (configuration 1).

different conditions were evaluated (flow rate, supply water temperature, etc.) to understand the sensibility of the system. By adopting a supply water temperature of 35 °C, once steady state conditions were achieved, heat flux trough the floor surface was around 25 W/m^2 and floor surface temperature was about 26 °C on average.

After the system was turned off, temperatures dropped down in 10 h once the phase change occurred in the containers. During the solidification of the hydrated salt (24 h), heat flux through the floor finishing surface was stable around 14 W/m^2 while the temperature of the floor surface was nearly 24 °C, and 27 °C at the top of the containers, on average. The significant amount of time required for the solidification process was mainly related to the absence of the fan.

According to Fig. 7, which outlines the cumulative frequency of heat flux in heating mode, the heat flux occurring due to the phase

change of the PCM would be able to cover heating energy needs for 20% of the cases, and of course for 24 h each time.

4.1.2. Wet sand condition

Time series of temperatures and heat fluxes for the wet sand condition are outlined in Figs. 16 and 17, which illustrate the scenario with a supply water temperature of 35 °C and 40 °C respectively. The lowest temperature was chosen for the comparison with the previous dry case, whilst the highest one was considered in order to achieve higher heat fluxes (for colder climates) and to check whether 35 °C was a thermal condition suitable to liquefy the whole PCM.

Compared to the scenario with dry sand and 35 °C supply water temperature, wet sand condition and fan operating allow to achieve a heat flux of about 40 W/m^2 in steady state, which is 60% higher than that in dry conditions. Once stopped the flow rate, temperatures dropped down in 6 h after the phase change occurred into the PCM containers; the shorter span should be mainly due to forced convection of the fan operating. During the solidification process of the hydrated salt (18 h) heat flux through the surface of the floor finishing was roughly stable around 28 W/m^2, whilst floor surface temperature was nearly 23 °C and almost 30 °C in PCM containers, on average.

As for the scenario with a supply water temperature of 40 °C, floor surface heat flux reached a value of 55 W/m^2 and floor surface temperature was almost 28 °C, very close to the threshold of 29 °C fixed by the standard regulation [17]. During the solidification phase (18 h), heat flux through the floor surface was around 30 W/m^2 whilst the temperature of the floor surface and temperature into the containers were similar to the previously investigated scenario.

4.1.3. Thermal performance

Based on the data reported in sections 4.1.1 and 4.1.2, it is possible to analyse the trends of heat flux through the floor surface in relation to the supply water temperature, therefore when the system is operating. The following graph (Fig. 18) illustrates the two cases of dry and wet sand conditions as reviewed above.

4.2. Experimental tests — configuration 2

4.2.1. Dry sand condition

Time series of temperatures and heat fluxes acquired for dry sand condition and the radiant floor configuration 2, i.e. with PCM containers installed under heating pipes, are illustrated in Fig. 19. After the first three days of non-stop operation, once steady state conditions were achieved, heat flux through floor finishing was about 40 W/m^2, while floor surface temperature was nearly 27.5 °C.

When the system was turned off the different temperatures dropped sharply in the following 9 h until the PCM started to solidify. Throughout the crystallisation process of the hydrated salt, which lasted almost 24 h, the average heat flux through floor finishing was 16 W/m^2, mean floor surface temperature was around 23 °C whilst temperature above containers was observed to be nearly 25.7 °C. The significant time needed for the PCM solidification was mainly due to the absence of the fan.

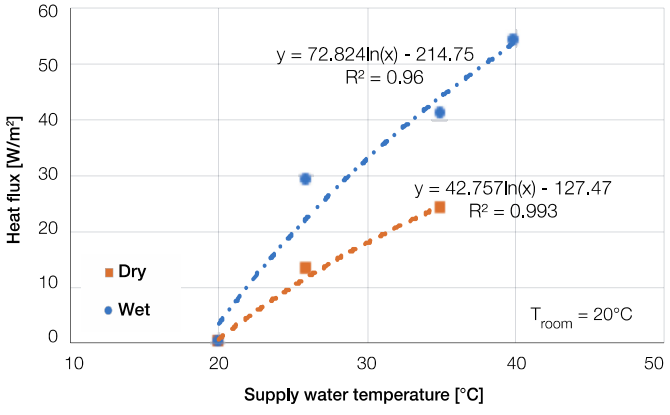

Fig. 18. Heat flux vs. working fluid temperature.

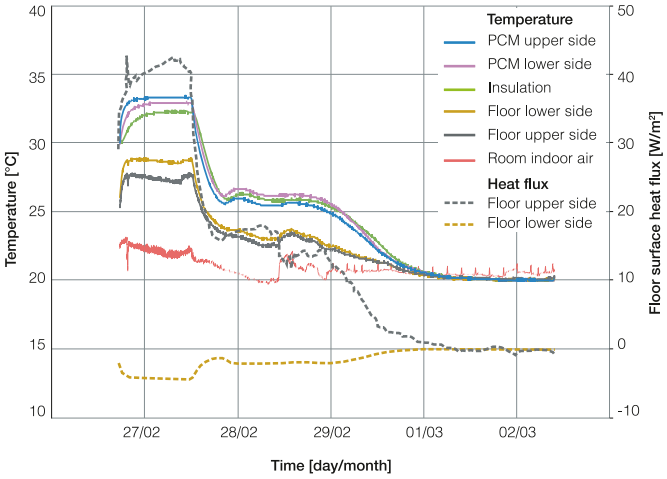

Fig. 19. Temperature distribution and heat flux in dry sand condition, 35 °C supply water temperature (configuration 2).

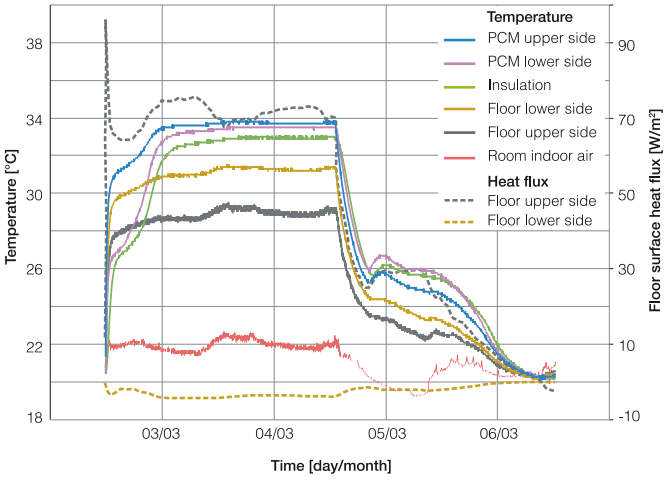

Fig. 20. Temperature distribution and heat flux in wet sand condition, 35 °C supply water temperature (configuration 2).

4.2.2. Wet sand condition

Time series of temperatures and heat fluxes acquired for the wet sand scenario are outlined in the following chart (Fig. 20). Taking into consideration steady state, heat flux through floor finishing was found to be almost 70 W/m^2, hence about 75% higher than in dry sand conditions. The mean floor surface temperature was nearly 28.5 °C. After the water flow rate was stopped, temperatures dropped in less than 8 h till the beginning of the crystallisation process of the hydrated salt, which took 15 h. Thus, the PCM started to solidify earlier and the transition phase lasted a shorter time compared to the dry sand scenario, mainly due to the forced convection generated by the fan. During PCM solidification mean heat

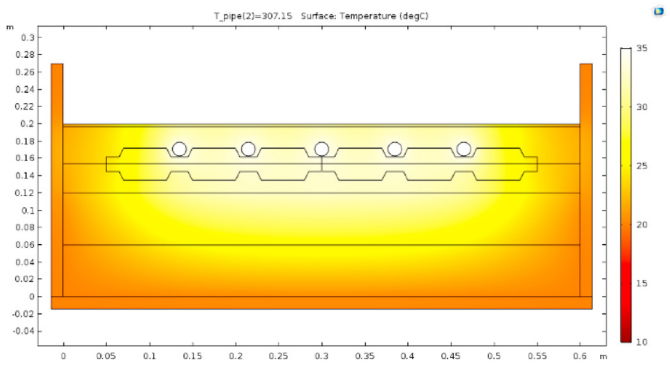

Fig. 21. Temperature distribution in steady state for wet sand condition.

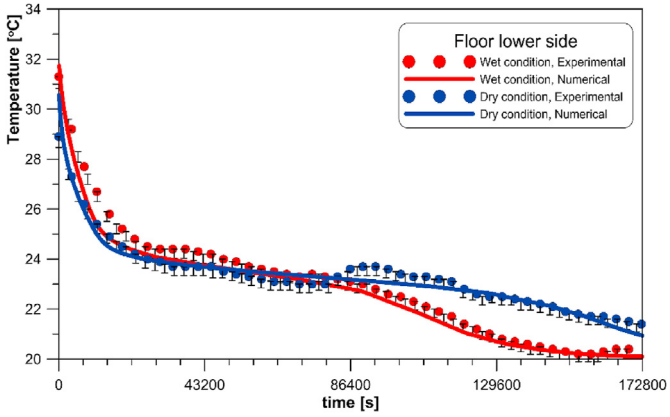

Fig. 22. Temporal changes of floor lower side temperature for dry and wet conditions.

flux through floor finishing was observed to be around 28 W/m^2, average floor surface temperature was a little lower than 23 °C while the temperature above containers was found to be almost 25 °C.

4.3. Numerical modelling – configuration 2

Temperature distribution in steady state obtained numerically in COMSOL Multiphysics® 5.5 [41] with a supply water temperature of 35 °C in the wet sand condition is illustrated in Fig. 21. The mean floor surface temperature for the dry sand condition was 27.5 °C and for the wet sand scenario was nearly 28.0 °C, which is the same and 0.5 °C lower than the value measured experimentally, respectively.

Temporal changes of temperature of the floor lower side acquired for dry and wet sand conditions are depicted in Fig. 22. These time series are related to the transient state when the water flow rate was stopped. As can be seen, values of temperature obtained numerically based on the model with 35 °C supply water temperature, marked as solid lines, are consistent with experimental values, marked as symbols, which allows to state that the developed model was correctly calibrated for both scenarios.

5. Conclusions and outlook

In the present study, the thermal behaviour of a hydronic radiant floor heating system enhanced with macroencapsulated PCM was analysed by means of numerical and experimental investigation. More in detail, temperature distribution and heat flux were examined in order to check the benefits of PCMs when off the heating system. The impact of using dry and wet sand, as well as the effect of the position of PCM containers – above or under heating pipes – on thermal performance, were investigated.

Experimental results showed that the use of high thermal conduction in mortar increases much faster the overall performance of the PCM integrated underfloor heating system in both the configurations examined. Indeed, taking into account the scenario with PCM containers installed above piping, it was found that heat flux in the wet sand condition was 60% higher than in dry sand when the system operated in steady state, and 100% higher than in dry sand when the transient mode was considered. Similarly, for the scenario with PCM containers installed under heating pipes, the use of wet sand allowed to achieve a heat flux through the floor surface 75% higher than the one reached by adopting dry sand. Moreover, the mean floor surface temperature for the wet sand condition was almost 1 °C higher than the dry sand condition.

The comparative analysis of the experimental results showed that configuration 2 with PCM containers installed under piping decisively contributes to the positive effect of wet sand on the thermal performance of the system. By adopting a supply water temperature of 35 °C in wet sand condition, macroencapsulated PCM positioned under heating pipes allows obtaining a floor surface heat flux about 75% higher than the one achieved in the PCM-under-pipes scenario. Furthermore, the floor surface temperature obtained with the system configuration 2 is nearly 1.5 °C higher than the temperature of the floor measured in configuration 1. In addition, once the phase change process occurred in the containers, temperatures dropped down in 8 h rather than 6 h as it was for configuration 1. The same strong positive contribution of PCM installed under heating pipes was found in Plytaria et al. [21], as reported in section 1.

The experimental analysis included the investigation of the scenario with a supply water temperature of 40 °C in wet sand for configuration 1, with the aim of examining the conditions for the achievement of higher heat fluxes for colder climates. However, much higher values of heat fluxes were obtained with a supply water temperature of 35 °C when PCM containers are installed under the piping. These findings suggested that the use of high thermal conduction in a mortar, along with the position of PCM under heating pipes, allow to optimise the temperature of supply water when higher heat fluxes are required.

The same thermal behaviour of the PCM integrated radiant floor heating system was reported by the results obtained from the numerical analysis, demonstrating that the numerical model was correctly calibrated for all the scenarios investigated.

In light of the results reviewed above, the validity and accuracy of the numerical models developed would allow conducting further analysis aimed at the design optimisation of the PCM enhanced radiant floor system in terms of both energy performance and thermal comfort. Indeed, the position of PCM containers under piping, along with the depth of heating pipes, pitch, water supply temperature, etc. can significantly impact not only on the energy performance of the system and the related energy consumption but also on the distribution of the floor surface temperature and therefore on the indoor thermal comfort of occupants.

Author statement

Barbara Larwa: Methodology, Software, Writing – original draft,

review & editing, Formal analysis, Supervision. Silvia Cesari: Writing – original draft, review & editing, Investigation, Formal analysis, Visualization. Michele Bottarelli: Conceptualization, Methodology, Software, Formal analysis, Validation, Funding acquisition.

Declaration of competing interest

The authors declare that they have no known competing financial interests or personal relationships that could have appeared to influence the work reported in this paper.

Acknowledgements

This work was supported financially within the IDEAS project – Novel building Integration Designs for increased Efficiencies in Advanced Climatically Tunable Renewable Energy Systems. This project is funded by the European Union's Horizon 2020 research and innovation programme under grant agreement No. 815271.

Nomenclature

Abbreviations

EPS	Expanded Polystyrene
FEM	Finite Element Method
HDPE	High-Density Polyethylene
HFM	Heat Flux Meter
HP	Heat Pump;
IDEAS	Novel building Integration Designs for increased Efficiencies in Advanced Climatically Tunable Renewable Energy Systems
ITES	Intra-day/season Thermal Energy Storage
LDPE	Low-Density Polyethylene
MES	Multi-source/sink Energy Sub-system
OSB	Oriented Strand Board
PCM	Phase Change Material
PE	Polyethylene
RES	Renewable Energy Systems
WP3	Work Package n.3

References

[1] European Environment Agency (EEA). Indicator assessment - data and maps - progress on energy efficiency in europe. 2019. Accessed 21st Feb 2021, https://www.eea.europa.eu/data-and-maps/indicators/progress-on-energy-efficiency-in-europe-3/assessment.
[2] Mohammadzadeh A, Kavgic M. Multivariable optimization of PCM-enhanced radiant floor of a highly glazed study room in cold climates. Build Simul 2020;13:559–74. https://doi.org/10.1007/s12273-019-0592-7.
[3] Yun BY, Yang S, Cho HM, Chang SJ, Kim S. Design and analysis of phase change material based floor heating system for thermal energy storage. Environ Res 2019;173:480–8. https://doi.org/10.1016/j.envres.2019.03.049.
[4] Lu S, Tong H, Pang B. Study on the coupling heating system of floor radiation and sunspace based on energy storage technology. Energy Build 2018;159:441–53. https://doi.org/10.1016/j.enbuild.2017.11.027.
[5] Karim L, Barbeon F, Gegout P, Bontemps A, Royon L. New phase-change material components for thermal management of the light weight envelope of buildings. Energy Build 2014;68:703–6. https://doi.org/10.1016/j.enbuild.2013.08.056.
[6] Royon L, Karim L, Bontemps A. Thermal energy storage and release of a new component with PCM for integration in floors for thermal management of buildings. Energy Build 2013;63:29–35. https://doi.org/10.1016/j.enbuild.2013.03.042.
[7] Cabrol L, Rowley P. Towards low carbon homes – a simulation analysis of building-integrated air-source heat pump systems. Energy Build 2012;48:127–36. https://doi.org/10.1016/j.enbuild.2012.01.019.
[8] Mazo J, Delgado M, Marin JM, Zalba B. Modeling a radiant floor system with Phase Change Material (PCM) integrated into a building simulation tool: analysis of a case study of a floor heating system coupled to a heat pump. Energy Build 2012;47:458–66. https://doi.org/10.1016/j.enbuild.2011.12.022.
[9] Jin P, Zhang X. Thermal analysis of a double layer phase change material floor. Appl Therm Eng 2011;31:1576–81. https://doi.org/10.1016/j.applthermaleng.2011.01.023.
[10] Qiu L, Liu X. Research on energy storage of building structure with phase change material. Jianzhu Cailiao Xuebao/Journal of Building Materials 2009;12:621–4.
[11] Zhang QL, Di HF, Lin KP, Zhang YP. Simulation on the thermal performance of hydraulic floor heating modular with shape-stabilized phase change materials for thermal energy storage. Kung Cheng Je Wu Li Hsueh Pao/Journal of Engineering Thermophysics 2006;27:641–3.
[12] Farid M, Kong WJ. Underfloor heating with latent heat storage. Proc IME J Power Energy 2001;215:601–9. https://doi.org/10.1243/0957650011538839.
[13] Yamaguchi M, Sayama S, Yoneda H, Iwamoto K, Harada M, Watanabe S, Fukai K. Heat storage-type floor heating system with heat pump driven by nighttime electric power. Heat Tran Jpn Res 1997;26(2):122–30. https://doi.org/10.1002/(SICI)1520-6556(1997)26:2<122::AID-HTJ6>3.0.CO;2-Y.
[14] Barrio M, Font J, Lopez DO, Muntasell J, Tamarit JL. Floor radiant system with heat storage by a solid-solid phase transition material. Sol Energy Mater Sol Cells 1992;27(2):127–33. https://doi.org/10.1016/0927-0248(92)90115-6.
[15] Zhou G, He J. Thermal performance of a radiant floor heating system with different heat storage materials and heating pipes. Appl Energy 2015;138:648–60. https://doi.org/10.1016/j.apenergy.2014.10.058.
[16] Baek S, Kim S. Analysis of thermal performance and energy saving potential by PCM radiant floor heating system based on wet construction method and hot water. Energies 2019;12(5):828. https://doi.org/10.3390/en12050828.
[17] EN 1264-2, water based surface embedded heating and cooling systems – Part 2: floor heating prove methods for the determination of the thermal output using calculation and test methods. 2008.
[18] Park J, Kim T. Analysis of the thermal storage performance of a radiant floor heating system with a PCM. Molecules 2019;24(7):1352. https://doi.org/10.3390/molecules24071352.
[19] Lu S, Xu B, Tang X. Experimental study on double pipe PCM floor heating system under different operation strategies. Renew Energy 2020;145:1280–91. https://doi.org/10.1016/j.renene.2019.06.086.
[20] Lu S, Gao J, Tong H, Yin S, Tang X, Jiang X. Model establishment and operation optimization of the casing PCM radiant floor heating system. Energy 2020;193:116814. https://doi.org/10.1016/j.energy.2019.116814.
[21] Plytaria MT, Tzivanidis C, Bellos E, Antonopoulos KA. Parametric analysis and optimization of an underfloor solar assisted heating system with phase change materials. Thermal Sci Eng Progress 2019;10:59–72. https://doi.org/10.1016/j.tsep.2019.01.010.
[22] Ascione F, Bianco N, de Masi RF, de' Rossi F, Vanoli GP. Energy refurbishment of existing buildings through the use of phase change materials: energy savings and indoor comfort in the cooling season. Appl Energy 2014;113:990–1007. https://doi.org/10.1016/j.apenergy.2013.08.045.
[23] Zhou D, Shire GSF, Tian Y. Parametric analysis of influencing factors in phase change material wallboard (PCMW). Appl Energy 2014;119:33–42. https://doi.org/10.1016/j.apenergy.2013.12.059.
[24] Ideas – novel building integration designs for increased efficiencies in advanced climatically tunable renewable energy systems. Accessed 21st Feb 2021, https://www.horizon2020ideas.eu.
[25] European Standard EN ISO 11855-2:2012. Building environment design - design, dimensioning, installation and control of embedded radiant heating and cooling systems - Part 2: Determination of the design heating and cooling capacity.
[26] Barreneche C, Navarro H, Serrano S, Cabeza LF, Fernández AI. New database on phase change materials for thermal energy storage in buildings to help PCM selection. Energy Procedia 2014;57:2408–15. https://doi.org/10.1016/j.egypro.2014.10.249.
[27] Cabeza LF, Castell A, Barreneche C, de Gracia A, Fernández AI. Materials used as PCM in thermal energy storage in buildings: a review. Renew Sustain Energy Rev 2011;15(3):1675–95. https://doi.org/10.1016/j.rser.2010.11.018.
[28] Lazaro A, Dolado P, Marin JM, Zalba B. PCM-air heat exchangers for free-cooling applications in buildings: empirical model and application to design. Energy Convers Manag 2009;50(3):444–9. https://doi.org/10.1016/j.enconman.2008.11.009.
[29] Ansuini R, Larghetti R, Giretti A, Lemma M. Radiant floors integrated with PCM for indoor temperature control. Energy Build 2011;43(11):3019–26. https://doi.org/10.1016/j.enbuild.2011.07.018.
[30] Butala V, Stritih U. Experimental investigation of PCM cold storage. Energy Build 2009;41(3):354359. https://doi.org/10.1016/j.enbuild.2008.10.008.
[31] Souayfane F, Fardoun F, Biwole PH. Phase change materials (PCM) for cooling applications in buildings: a review. Energy Build 2016;129:396–431. https://doi.org/10.1016/j.enbuild.2016.04.006.
[32] PCM Products Ltd. Accessed 21st Feb 2021, http://www.pcmproducts.net.
[33] Thermtest. Materials thermal properties database. Available at. Accessed 21st Feb 2021, https://thermtest.com/materials-database.
[34] UNI 11466:2012, Sistemi geotermici a pompa di calore - requisiti per il dimensionamento e la progettazione. UNI; 2012 [In Italian)].
[35] PCM Products Ltd. PlusICE hydrated salt (S) range. 2018. Accessed 21st Feb 2021, http://www.pcmproducts.net/files/S%20range-2018.pdf.
[36] Bortolo Fassa. EPS 120 insulation board datasheet (In Italian) [Accessed 21st 2021], https://www.fassabortolo.it/documents/10179/554550/FASSA_STE_IT_LASTRA-ISOLANTE-IN-EPS-120_2019-03.pdf/9fb66a9a-5129-4288-be7b-f9441a05ec41.

[37] Thermo Scientific™ ARCTIC A25 refrigerated circulators. Accessed 21st Feb 2021, https://www.thermofisher.com/order/catalog/product/156-5258?SID=srch-srp-156-5258#/156-5258?SID=srch-srp-156-5258.
[38] Ahlborn. Heat flow, heat flow plates FQAx. Accessed 21st Feb 2021, https://www.ahlborn.com/download/pdfs/kap13/eng/WflPlatte.pdf.
[39] Delta strumenti, thermocouple wire (in Italian). Accessed 21st Feb 2021, https://www.deltastrumenti.it/images/pdf/termocoppie/in_cavetto/Termocoppia_cavetto.pdf.
[40] Ahlborn. Input connectors and adapter cables, ALMEMO® connector for thermocouple types K, N, J, T. Accessed 21st Feb 2021, https://www.ahlborn.com/download/pdfs/kap02/eng/Thermoe.pdf.
[41] Ahlborn. Data acquisition system ALMEMO® 5690-2M. Accessed 21st Feb 2021, https://www.ahlborn.com/download/anleitung/eng/56902e.pdf.
[42] COMSOL Multiphysics® v. 5.5, COMSOL AB, stockholm, Sweden. www.comsol.com.
[43] Phase change. COMSOL Model Library; 2012.
[44] Bottarelli M, Di Federico V, Fujii H. Performance of a drainage trench employed as ground heat exchanger. In: Proceedings of the 15th international heat transfer conference, kyoto; 2014. https://doi.org/10.1615/IHTC15.pmd.009937.
[45] Bottarelli M, Bortoloni M, Su Y. Heat transfer analysis of underground thermal energy storage in shallow trenches filled with encapsulated phase change materials. Appl Therm Eng 2015;90:1044–51. https://doi.org/10.1016/j.applthermaleng.2015.04.002.